Journal of Visual Communication and Image Representation **13**, 3–21 (2002)
doi:10.1006/jvci.2001.0482, available online at http://www.idealibrary.com on IDEAL®

Dense Disparity Map Estimation Respecting Image Discontinuities: A PDE and Scale-Space Based Approach

Luis Alvarez

Departamento de Informática y Sistemas, Universidad de Las Palmas, Campus de Tafira, SP-35017 Las Palmas, Spain
E-mail: lalvarez@dis.ulpgc.es
URL: http://serdis.dis.ulpgc.es/∼lalvarez

Rachid Deriche

INRIA Sophia-Antipolis, 2004, Route des Lucioles, F-06902 Sophia-Antipolis, France
E-mail: Rachid.Deriche@sophia.inria.fr
URL: http://www-sop.inria.fr/robotvis/personnel/der

Javier Sánchez

Departamento de Informática y Sistemas, Universidad de Las Palmas, Campus de Tafira, SP-35017 Las Palmas, Spain
E-mail: jsanchez@dis.ulpgc.es
URL: http://serdis.dis.ulpgc.es/∼jsanchez

and

Joachim Weickert

Computer Vision, Graphics, and Pattern Recognition Group, Department of Mathematics and Computer Science, University of Mannheim, D-68131 Mannheim, Germany
E-mail: Joachim.Weickert@uni-mannheim.de
URL: http://www.cvgpr.uni-mannheim.de/weickert

Received January 26, 2000; accepted August 7, 2000

We present an energy based approach to estimate a dense disparity map from a set of two weakly calibrated stereoscopic images while preserving its discontinuities resulting from image boundaries. We firs derive a simplifie expression for the disparity that allows us to estimate it from a stereo pair of images using an energy minimization approach. We assume that the epipolar geometry is known, and we include this information in the energy model. Discontinuities are preserved by means of a regularization term based on the Nagel–Enkelmann operator. We investigate the associated Euler–Lagrange equation of the energy functional, and we approach the solution of the underlying partial differential equation (PDE) using a gradient descent method. The resulting parabolic problem has a unique solution. In order to reduce the risk to be trapped within some irrelevant local minima during the iterations, we

1047-3203/02 $35.00

use a focusing strategy based on a linear scale-space. Experimental results on both synthetic and real images are presented to illustrate the capabilities of this PDE and scale-space based method.

Key Words: stereoscopic vision; disparity map; anisotropic diffusion; scale-space; partial differential equations; regularization; f nite difference methods.

1. INTRODUCTION

The goal of this paper is to present a variational approach to recover a dense disparity map from a set of two weakly calibrated stereoscopic images. To solve this problem, we f rst make full use of the knowledge of the so-called fundamental matrix [15] to derive the equations that relate corresponding pixels in the two views. Then we combine regularization and scale-space tools to estimate iteratively and hierarchically the disparity map. The solution obtained at a coarse spatial scale is used to restrict searching at f ner scales. We minimize an energy term that takes into account the epipolar line constraint as well as the edge information constraint through an appropriate regularization term.

Over the years, numerous algorithms for stereo vision have been proposed, which use different strategies.

- **Feature based:** These algorithms establish correspondences between some selected features extracted from the images [15, 22], such as edge pixels [37, 38], line segments [6, 29, 30], or curves [10, 33, 43]. Their main advantage is to yield accurate information and to manipulate reasonably small amounts of data, thus gaining in time and space complexity. Their main drawback is the sparseness of the recovered depth information. This class of methods was widely used some years ago, when it was not possible to retrieve a dense and accurate reconstruction within a reasonable amount of time.
- **Area based:** In these approaches, dense depth maps are provided by correlating the gray levels of image patches in the views being considered, assuming that they present some similarity [13, 15, 16, 21, 36]. These methods are well adapted for relatively textured areas; however, they generally assume that the observed scene is locally fronto-parallel, which causes problems for slanted surfaces and in particular near the occluding contours of the objects. Last, the matching process does not take into account the edge information which is actually very important information that should be used in order to get reliable and accurate dense maps.
- **Phase based:** Another class of methods is based on the Fourier phase information, which can be considered as a sort of gradient-based optical f ow method, with the time derivative approximated by the difference between the left and right Fourier phase images [18, 19, 25, 27, 52]. Hierarchical methods are also used here in order not to get trapped in some local minimum.
- **Energy based:** A last kind of approach which does not suffer from any of the shortcomings presented above consists of solving the correspondence problem in a minimization and regularization formulation [7, 9, 11, 12, 17, 23, 40–42, 46, 53]. An iterative solution of the discrete version of the associated Euler–Lagrange equation is then used in order to estimate disparity or depth.

For instance, in [42], a variational approach for solving the stereo problem was proposed using the classical quadratic Tikhonov regularization term in order to obtain a smooth depth

map. This work has been extended in [41] where the authors propose a method to directly compute the depth map $Z(x, y)$ between two images I_l and I_r as the minimum of the following energy

$$S(Z) = \iint (I_l(x, y) - I_r(f(x, y, Z(x, y)))^2 \, dx \, dy + \nu \iint \Phi(|\nabla Z|) \, dx \, dy, \quad (1)$$

where $f(.,.,.)$ depends on the camera intrinsic and extrinsic parameters derived from an off-line calibration step, and where the regularization function $\Phi(\cdot)$ is no more a quadratic function but specif cally designed to preserve possible discontinuities in the depth map. The minimum of the above energy is calculated using the associated Euler–Lagrange equation.

In [17], a different variational stereo approach is presented. It works for two or more images. The deduced Euler–Lagrange equations provide a set of PDEs which are used to deform an initial set of surfaces toward the objects to be detected while taking into account the orientation of the tangent plane to the object. This approach can be seen as a 3D extension of the approach in [11, 12] where just the binocular case has been studied to f nd cross-sections of the objects with a f xed plane. Note that these references require a set of strongly calibrated images and that they use a level set implementation of the PDEs to provide a surface or curve evolution that deals automatically with changes in topology.

The method we present in this paper is also energy based, but it has not much in common with [17]. It can be considered as a generalization of the work in [41] to the weakly calibrated case, with the following important originalities:

- As has been already said, the method presented in this article considers a weakly calibrated stereoscopic system, i.e., the stereoscopic system is not calibrated, as in [41], and only the knowledge of the so-called fundamental matrix is known. The intrinsic and extrinsic parameters of the camera are not known.
- Consequently, one computes a sort of projective depth directly related to the well-known disparity measure from the gray level images intensities, while in [41], the authors directly estimate the depth information. We do not have to deal with any intermediate process such as rectif cation [5, 39, 44, 54]. The projective depth information is directly issued as a function $m \to D(m)$ of the image point.
- This method addresses the problem of accurately determining the dense disparity map while regularizing it along the contours of the gray level image and inhibiting smoothing across the image discontinuities. In [41], the regularization process was performed in order to inhibit smoothing the depth map at the estimated depth discontinuities. On the other hand, in $S(Z)$ the preservation of discontinuities in the depth Z is obtained by the nonlinear diffusion operator associated to the function Φ, while in our method, the preservation of discontinuities in the disparity map is obtained using an anisotropic linear operator which allows us to develop discontinuities in the disparity map across the edges of the image I_l. This is achieved by considering a Nagel–Enkelmann regularization term that has already proven its usefulness in optical f ow estimation [3, 32].
- Another important item is related to the way we proceed in order to avoid convergence to irrelevant minima. A focusing strategy embedding the method in a linear scale-space is used, as it has already been successfully applied in optical f ow estimation [3, 4].

This also relates our work to stereo methods using linear scale-space such as [26, 28, 34, 35].

The paper is organized as follows: In Section 2, we present the formalism of the matching process and discuss all relevant features of our model. In Section 3 we discuss numerical aspects of our algorithm, and in Section 4 we present experimental results. Finally, we conclude with a summary in Section 5. In order to focus on the novelty of our algorithm in the context of stereoscopic vision, we can only brief y survey those features that are described in more detail in our related work on optic f ow estimation [4].

2. FORMALISM OF THE MATCHING PROCESS

2.1. Notation and Background

In this paper we use a projective camera model (Fig. 1). This model maps a 3D point $\mathbf{M} = [X, Y, Z]^t$ to a 2D image point $\mathbf{m} = [x, y]^t$ through a 3×4 projection matrix $\mathbf{P}$ via $s\hat{\mathbf{m}} = \mathbf{P}\hat{\mathbf{M}}$, where s is a nonzero scale factor and the notation $\hat{\mathbf{p}}$ is such that if $\mathbf{p} = [x, y, \ldots]^t$ then $\hat{\mathbf{p}} = [x, y, \ldots, 1]^t$. In the case of two images acquired by a binocular stereo system, every physical point $\mathbf{M}$ in space yields a pair of 2D projections $\mathbf{m_1}$ and $\mathbf{m_2}$ on the two images. The 3×4 projection matrices are def ned by the following relations:

$$s_1\hat{\mathbf{m}}_1 = \mathbf{P_1}\hat{\mathbf{M}}, \qquad s_2\hat{\mathbf{m}}_2 = \mathbf{P_2}\hat{\mathbf{M}}. \tag{2}$$

Assuming that the world coordinate system is associated with the f rst camera, the two projection matrices are given by

$$\mathbf{P_1} = [\mathbf{A}|\mathbf{0}], \qquad \mathbf{P_2} = [\mathbf{A}'\mathbf{R} \,|\, \mathbf{A}'\,\mathbf{t}], \tag{3}$$

where $\mathbf{R}$ and $\mathbf{t}$ represent the 3×3 rotation matrix and the 3×1 translation vector def ning the rigid displacement between the two cameras, and $\mathbf{0}$ denotes the 3×1

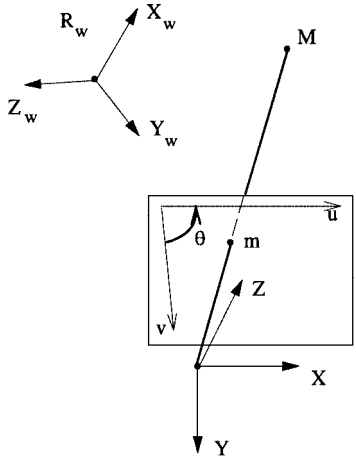

FIG. 1. The pinhole model and the different frames.

null vector. The matrices $\mathbf{A}$ and $\mathbf{A}'$ are the 3×3 intrinsic parameters matrices of the two views, each depending on five parameters and having the following well-known form [15]:

$$\mathbf{A} = \begin{bmatrix} \alpha_u & -\alpha_u \cot\theta & u_0 \\ 0 & \alpha_v/\sin\theta & v_0 \\ 0 & 0 & 1 \end{bmatrix}, \qquad \mathbf{A}' = \begin{bmatrix} \alpha'_u & -\alpha'_u \cot\theta' & u'_0 \\ 0 & \alpha'_v/\sin\theta' & v'_0 \\ 0 & 0 & 1 \end{bmatrix}. \tag{4}$$

The parameters α_u(resp. α'_u) and α_v(resp. α'_v) correspond to the focal distances in pixels along the axes of the image, θ(resp. θ') is the angle between the two image coordinate axes, and (u_0, v_0) (resp. (u'_0, v'_0)) are the coordinates of the image principal point. The ratio α_v/α_u(resp. $\alpha'_v/\alpha_{u'}$) is known as the *aspect ratio*. When both images have been acquired by the same camera, $\theta = \theta'$ and $\frac{\alpha_v}{\alpha_u} = \frac{\alpha_{v'}}{\alpha_{u'}}$, even if the focal lengths have changed. In practice, θ and θ' are very close to $\frac{\pi}{2}$ for real cameras [15]. Additionally, modern cameras have almost square pixels, therefore in this case the aspect ratio is very close to 1.

All these matrices and parameters can be computed with good accuracy by means of a classical calibration method [15]. In such a case, the system is said to be *calibrated*.

By eliminating the scalars s_1 and s_2 associated with the projection equations (2) as well as the point $\mathbf{M}$, an equation relating the pair of projections of the same 3D point is obtained:

$$\hat{\mathbf{m}}_\mathbf{2}{}^t \mathbf{F} \hat{\mathbf{m}}_\mathbf{1} = 0. \tag{5}$$

In this equation, the matrix $\mathbf{F}$ is the fundamental matrix, given by

$$\mathbf{F} = \mathbf{A}'^{*}[\mathbf{t}]_\times \mathbf{R} \mathbf{A}^{-\mathbf{1}}, \tag{6}$$

where $\mathbf{A}'^{*} = (\mathbf{A}'^{-\mathbf{1}})^t$ is the adjoint matrix of $\mathbf{A}'$, and $[\mathbf{x}]_\times$ denotes the antisymmetric matrix of vector $\mathbf{x}$ that is associated with the cross product. This matrix has the property $[\mathbf{x}]_\times \mathbf{y} = \mathbf{x} \times \mathbf{y}$ for each vector $\mathbf{y}$ and has the following analytic form:

$$[\mathbf{x}]_\times = \begin{bmatrix} 0 & -x_3 & x_2 \\ x_3 & 0 & -x_1 \\ -x_2 & x_1 & 0 \end{bmatrix}. \tag{7}$$

For a point $\mathbf{m_1} = [x, y]^t$ in the first image I_l, the fundamental matrix $F = (f_{i,j})$ provides the epipolar line Δ of equation $\hat{\mathbf{m}}_\mathbf{2}{}^t \mathbf{F} \hat{\mathbf{m}}_\mathbf{1} = 0$ in the image I_r. Let us introduce the notation

$$a(x, y) := f_{11}x + f_{12}y + f_{13}, \tag{8}$$

$$b(x, y) := f_{21}x + f_{22}y + f_{23}, \tag{9}$$

$$c(x, y) := f_{31}x + f_{32}y + f_{33}. \tag{10}$$

Using this notation, the epipolar line Δ can be written as

$$a(x, y)x' + b(x, y)y' + c(x, y) = 0. \tag{11}$$

We will use this equation in order to introduce our specific parameterization of the disparity, developed to yield a simple linear second order differential operator in the minimization part.

2.2. The Disparity Term

Under the Lambertian assumption that corresponding pixels have equal gray values, the determination of the disparity from the stereo pair comes down to finding a function $\mathbf{h}(x, y) := (u(x, y), v(x, y))^t$ such that

$$I_l(x, y) = I_r(x + u(x, y), y + v(x, y)), \qquad \forall (x, y) \in \mathbb{R}^2, \tag{12}$$

where the point $(x', y') = (x + u(x, y), y + v(x, y))$ belongs to the epipolar line associated to (x, y).

Let us denote by $\mathbf{N}$ (resp. $\mathbf{T}$) the unitary normal (resp. tangential) vector of the epipolar line Δ given by the equation $\hat{\mathbf{m}}_\mathbf{2}{}^t \mathbf{F} \hat{\mathbf{m}}_\mathbf{1} = 0$, and by $\mathbf{D}$ the unitary disparity vector associated to the points $\mathbf{m_1}$ and $\mathbf{m_2}$:

$$\mathbf{N} = \begin{bmatrix} \frac{a}{\sqrt{a^2+b^2}} \\ \frac{b}{\sqrt{a^2+b^2}} \end{bmatrix}; \qquad \mathbf{T} = \begin{bmatrix} \frac{-b}{\sqrt{a^2+b^2}} \\ \frac{a}{\sqrt{a^2+b^2}} \end{bmatrix}; \qquad \mathbf{D} = \begin{bmatrix} \frac{u}{\sqrt{u^2+v^2}} \\ \frac{v}{\sqrt{u^2+v^2}} \end{bmatrix}. \tag{13}$$

Then we have

$$\mathbf{m_2} = \mathbf{m_1} + \delta \mathbf{D} = \mathbf{m_1} - \gamma \mathbf{N} - \lambda \mathbf{T}, \tag{14}$$

where $\delta = \sqrt{u^2 + v^2}$ represents the disparity, and

$$\gamma = \frac{\hat{\mathbf{m}}_\mathbf{1}{}^t \mathbf{F} \hat{\mathbf{m}}_\mathbf{1}}{\sqrt{a^2 + b^2}} \tag{15}$$

is the distance (modulus a sign) of the point $\mathbf{m_1}$ to its epipolar line Δ in the second image. The function λ represents the distance (modulus a sign) of $\mathbf{m_0}$, the projection of the point $\mathbf{m_1}$ on the epipolar line Δ, to the point $\mathbf{m_2}$ that lies along the epipolar line Δ.

Using these equations, one can easily derive the following expression for the disparity components,

$$u(x, y) = \frac{-\lambda(x, y) b(x, y)}{\sqrt{a^2(x, y) + b^2(x, y)}} - \frac{a(x, y)x + b(x, y)y + c(x, y)}{a^2(x, y) + b^2(x, y)} a(x, y), \tag{16}$$

$$v(x, y) = \frac{\lambda(x, y) a(x, y)}{\sqrt{a^2(x, y) + b^2(x, y)}} - \frac{a(x, y)x + b(x, y)y + c(x, y)}{a^2(x, y) + b^2(x, y)} b(x, y), \tag{17}$$

where $\lambda(x, y)$ represents a parameter associated to the depth of the physical point considered. In what follows, we use the notation $\mathbf{h}(\lambda(x, y)) = (u(\lambda(x, y)), v(\lambda(x, y)))$ to indicate that the disparity depends on the single parameter $\lambda(x, y)$. Note that $\lambda(x, y) = 0$ provides the point of the epipolar line which minimizes the distance between the epipolar line and the

point (x, y). Using the epipolar constraint and noting that $\gamma(x, y)$ is known for each point (x, y) thanks to the knowledge of the fundamental matrix, the computation of the disparity map $\delta(x, y)$ can be reduced to the computation of the single function $\lambda(x, y)$:

$$\delta(x, y)^2 = \lambda(x, y)^2 + \gamma(x, y)^2. \tag{18}$$

2.3. The Energy Functional

Let us now develop an approach to accurately estimate the $\lambda(x, y)$ function associated to a pair of stereoscopic images. The easiest possibility would be to proceed in a classical way and try to recover this important information using a simple correlation scheme. Unfortunately, this naive solution will not provide a correct and accurate result, in particular in the regions where the disparity map has discontinuities, as is often the case at image edges. It is well known that the disparity map of this classical method tends to be very smooth across the image boundaries. The idea we would like to formalize and develop here is to estimate a $\lambda(x, y)$ function which is smooth only along the image boundaries and not across them. This leads us to consider the minimization of the following energy functional:

$$\begin{aligned} E(\lambda) = &\int_\Omega (I_l(x, y) - I_r(x + u(\lambda(x, y)), y + v(\lambda(x, y))))^2 \, dx \, dy, \\ &+ C \int_\Omega \nabla\lambda^t D(\nabla I_l) \nabla\lambda \, dx \, dy. \end{aligned} \tag{19}$$

Here, Ω denotes the image domain, C is a positive constant, and $D(\nabla I_l)$ is a regularized projection matrix perpendicular to ∇I_l,

$$D(\nabla I_l) = \frac{1}{|\nabla I_l|^2 + 2\nu^2} \left\{ \begin{bmatrix} \frac{\partial I_l}{\partial y} \\ -\frac{\partial I_l}{\partial x} \end{bmatrix} \begin{bmatrix} \frac{\partial I_l}{\partial y} \\ -\frac{\partial I_l}{\partial x} \end{bmatrix}^t + \nu^2 \, Id \right\}, \tag{20}$$

where Id denotes the identity matrix. This projection has been introduced by Nagel and Enkelmann [31, 32] in the context of optic f ow estimation. We use it here because of its simplicity (the underlying second order differential operator is linear) and because this method has demonstrated its performance numerous times in the context of optical f ow estimations [3, 4, 8, 14, 31, 32, 45, 47].

2.4. Minimizing the Energy

In order to minimize our energy functional, we solve its associated Euler–Lagrange equation

$$C \operatorname{div}(D(\nabla I_l)\nabla\lambda) + \big(I_l(\mathbf{x}) - I_r^\lambda(\mathbf{x})\big) \frac{a \left(\frac{\partial I_r}{\partial y}\right)^\lambda (\mathbf{x}) - b \left(\frac{\partial I_r}{\partial x}\right)^\lambda (\mathbf{x})}{\sqrt{a^2 + b^2}} = 0, \tag{21}$$

where $\mathbf{x} := (x, y)^t$, $I_r^\lambda(\mathbf{x}) := I_r(\mathbf{x} + \mathbf{h}(\lambda(\mathbf{x})))$, and $(\partial I_r/\partial x)^\lambda(\mathbf{x}) := \partial I_r/\partial x(\mathbf{x} + \mathbf{h}(\lambda(\mathbf{x})))$. We obtain a solution of the above equation by calculating the asymptotic state ($t \to \infty$) of

the parabolic equation

$$\frac{\partial \lambda}{\partial t} = C\,\mathrm{div}(D(\nabla I_l)\nabla\lambda) + \big(I_l(\mathbf{x}) - I_r^{\lambda}(\mathbf{x})\big)\frac{a\left(\frac{\partial I_r}{\partial y}\right)^{\lambda}(\mathbf{x}) - b\left(\frac{\partial I_r}{\partial x}\right)^{\lambda}(\mathbf{x})}{\sqrt{a^2+b^2}}. \tag{22}$$

We observe that in this diffusion-reaction method the matrix $D(\nabla I_l)$ plays the role of a diffusion tensor. Its eigenvectors are $v_1 := \nabla I_l$ and $v_2 := \nabla I_l^{\perp}$, and the corresponding eigenvalues are given by

$$\lambda_1(|\nabla I_l|) = \frac{\nu^2}{|\nabla I_l|^2 + 2\nu^2}, \qquad \lambda_2(|\nabla I_l|) = \frac{|\nabla I_l|^2 + \nu^2}{|\nabla I_l|^2 + 2\nu^2}. \tag{23}$$

In the interior of objects we have $|\nabla I_l| \to 0$, and therefore $\lambda_1 \to 1/2$ and $\lambda_2 \to 1/2$. At ideal edges where $|\nabla I_l| \to \infty$, we obtain $\lambda_1 \to 0$ and $\lambda_2 \to 1$. Thus, we have isotropic behavior within regions, and at image boundaries the process smoothes anisotropically along the edge. This behavior is very similar to edge-enhancing anisotropic diffusion f ltering [49, 50], and it is also close in spirit to the modif ed mean-curvature motion considered in [2].

2.5. A Linear Scale-Space Approach to Recover Large Disparities

In general, the Euler–Lagrange equation (21) will have multiple solutions. As a consequence, the asymptotic state of the parabolic equation (22), which we use for approximating the disparity, will depend on the initial data. Typically, we may expect that the algorithm converges to a local minimizer of the energy functional (19) that is located in the vicinity of the initial data. To avoid convergence to irrelevant local minima, we embed our method into a linear scale-space framework [24, 51]. For recent detailed descriptions of linear scale-space theory we refer to [20, 48]. Considering the problem at a coarse scale avoids that the algorithm gets trapped in physically irrelevant local minima.

The basic idea of embedding our method in linear scale-space is as follows [3]: we replace the images I_l and I_r in (22) by $I_l^{\sigma} := G_\sigma * I_l$ and $I_r^{\sigma} := G_\sigma * I_r$, where $*$ is the convolution operator, and G_σ denotes a Gaussian with standard deviation σ. We start with a large initial scale σ_0. Then we compute the disparity λ_{σ_0} at scale σ_0 as the asymptotic state of the solution using some initial approximation (see below). Next, we choose a number of scales $\sigma_n < \sigma_{n-1} < \cdots < \sigma_0$, and for each scale σ_i we compute the disparity λ_{σ_i} as the asymptotic state of the above PDE with initial data $\lambda_{\sigma_{i-1}}$. The f nal disparity corresponds to the smallest scale σ_n. In accordance with the logarithmic sampling strategy in linear scale-space theory, we choose $\sigma_i := \eta^i \sigma_0$ with some decay rate $\eta \in (0, 1)$. A detailed analysis of the usefulness of such a focusing strategy in the context of a related optic f ow problem can be found in [4].

Our method is governed by the evolution equation

$$\frac{\partial \lambda_\sigma}{\partial t} = C\,\mathrm{div}\big(D\big(\nabla I_l^{\sigma}\big)\nabla\lambda_\sigma\big) + \big(I_l^{\sigma}(\mathbf{x}) - I_r^{\sigma,\lambda_\sigma}(\mathbf{x})\big)\frac{a\left(\frac{\partial I_r^{\sigma}}{\partial y}\right)^{\lambda_\sigma}(\mathbf{x}) - b\left(\frac{\partial I_r^{\sigma}}{\partial x}\right)^{\lambda_\sigma}(\mathbf{x})}{\sqrt{a^2+b^2}}. \tag{24}$$

For the initial value $\lambda_0^{\sigma_0}(x, y)$ we consider two possibilities. The first one is to take a constant value which depends, in general, on a rough a priori estimation of the expected disparity, following an estimation of the depth where the interesting objects are located. Another possibility is to use the result of a simple classic method for estimating the disparity, for instance a correlation technique.

Equation (24) leads to a mathematically correct concept: in [1] we have shown that if I_l, I_r and the initial data λ_σ^0 belong to $L^2(\mathbb{R}^2)$, then there exists a unique generalized solution $\lambda_\sigma(t) \in C([0, \infty); L^2(\mathbb{R}^2))$.

2.6. *Invariance under Linear Gray Value Transformations*

A remaining shortcoming of the modified model is that the energy functional is not invariant under gray level transformation of the form $(I_l, I_r) \to (kI_l, kI_r)$, where k is a constant. Therefore, the choice of the parameters depends strongly on the image contrast. This is especially problematic when the method is embedded in the scale-space focusing strategy, since the amount of smoothing influences the contrast range in the regularized images I_l^σ and I_r^σ.

Our recent optic flow research [4] showed that this problem can be solved as follows. We compute C and ν by specifying two parameters $\alpha, s \in (0, 1)$ such that

$$C = \frac{\alpha}{\max_{\mathbf{x}}\left(\left|\left(\nabla I_l^\sigma\right)(\mathbf{x})\right|^2\right)}, \qquad s = \int_0^\nu \mathcal{H}_{|\nabla I_l^\sigma|}(z)\, dz, \tag{25}$$

where $\mathcal{H}_{|\nabla I_l^\sigma|}(z)$ represents the normalized histogram of $|\nabla I_l^\sigma|$. We name s the isotropy fraction. When $s \to 0$, the diffusion operator becomes anisotropic at all locations, and when $s \to 1$, it leads to isotropic diffusion everywhere. In practical applications of our method it is thus sufficient to specify the parameters α and s instead of C and ν. The parameters C and ν are then automatically adjusted to the dynamic image range in each step of the focusing procedure.

3. NUMERICAL SCHEME

Next we describe an efficient algorithm for our model. We discretize the parabolic equation (24) by finite differences. All spatial derivatives are approximated by central differences, and for the discretization in t direction we use a linear implicit scheme. Let $D(\nabla I_l^\sigma) =: \left(\begin{smallmatrix} d & f \\ f & e \end{smallmatrix}\right)$. Then our linear implicit scheme has the structure

$$\begin{aligned}
\frac{\lambda_{i,j}^{k+1} - \lambda_{i,j}^{k}}{\tau} = C \Bigg(& \frac{d_{i+1,j} + d_{i,j}}{2} \frac{\lambda_{i+1,j}^{k+1} - \lambda_{i,j}^{k+1}}{h_1^2} + \frac{d_{i-1,j} + d_{i,j}}{2} \frac{\lambda_{i-1,j}^{k+1} - \lambda_{i,j}^{k+1}}{h_1^2} \\
& + \frac{f_{i,j+1} + f_{i,j}}{2} \frac{\lambda_{i,j+1}^{k+1} - \lambda_{i,j}^{k+1}}{h_2^2} + \frac{f_{i,j-1} + f_{i,j}}{2} \frac{\lambda_{i,j-1}^{k+1} - \lambda_{i,j}^{k+1}}{h_2^2} \\
& + \frac{e_{i+1,j+1} + e_{i,j}}{2} \frac{\lambda_{i+1,j+1}^{k+1} - \lambda_{i,j}^{k+1}}{2h_1h_2} + \frac{e_{i-1,j-1} + e_{i,j}}{2} \frac{\lambda_{i-1,j-1}^{k+1} - \lambda_{i,j}^{k+1}}{2h_1h_2} \\
& - \frac{e_{i+1,j-1} + e_{i,j}}{2} \frac{\lambda_{i+1,j-1}^{k+1} - \lambda_{i,j}^{k+1}}{2h_1h_2} - \frac{e_{i-1,j+1} + e_{i,j}}{2} \frac{\lambda_{i-1,j+1}^{k+1} - \lambda_{i,j}^{k+1}}{2h_1h_2} \Bigg)
\end{aligned}$$

$$+\left(I_l(\mathbf{x}_{i,j}) - I_r^{\lambda_{i,j}^k}(\mathbf{x}_{i,j}) - \frac{\lambda_{i,j}^{k+1} - \lambda_{i,j}^k}{\sqrt{a_{i,j}^2 + b_{i,j}^2}}\left(a_{i,j} I_{r,y}^{\lambda_{i,j}^k}(\mathbf{x}_{i,j}) - b_{i,j} I_{r,x}^{\lambda_{i,j}^k}(\mathbf{x}_{i,j})\right)\right)$$

$$\cdot \frac{a_{i,j} I_{r,y}^{\lambda_{i,j}^k}(\mathbf{x}_{i,j}) - b_{i,j} I_{r,x}^{\lambda_{i,j}^k}(\mathbf{x}_{i,j})}{\sqrt{a_{i,j}^2 + b_{i,j}^2}}, \tag{26}$$

where τ is the time step size, h_1 and h_2 denote the pixel size in x and y directions, respectively, $\lambda_{i,j}^k$ approximates λ_σ in some grid point $\mathbf{x}_{i,j}$ at time $k\tau$, and $I_{r,x}^{\lambda_{i,j}^k}(\mathbf{x}_{i,j})$ is an approximation to $\partial I_r^{\sigma,\lambda}/\partial_x\,(\mathbf{x}_{i,j}, \boldsymbol{k}\tau)$. We calculate values outside grid points by linear interpolation, and we solve the resulting linear system of equations iteratively by a symmetric Gauß–Seidel algorithm [4].

The linear implicit scheme offers the advantage of using large time steps in order to accelerate convergence to the steady state. We use the step size $\tau = 10$ and stop the process after 50 iterations.

4. EXPERIMENTAL RESULTS

In our f rst experiment we use a classical synthetic stereo pair where the exact disparity is known. In this case the epipolar lines are parallel to the horizontal axis, and the fundamental matrix F is given by

$$F = \begin{bmatrix} 0 & 0 & 0 \\ 0 & 0 & 1 \\ 0 & -1 & 0 \end{bmatrix}. \tag{27}$$

We compute the error as the average absolute value of the difference between the computed disparity with the exact disparity. In order to avoid the image boundary inf uence we do not take into account a boundary layer of 15 pixels.

We compare our method with an improved version of the classical correlation technique, where we use some interpolation techniques in order to get subpixel precision as well as a 100% disparity map. With this correlation technique, we found out that, concerning the disparity error, the best window size is 23×23. For this window size the error is 0.4978.

Table 1 shows the results obtained using our method for different parameter settings, and in Fig. 2 we present the best result that we have obtained with our method. It has an average error of 0.2639. Table 1 also shows that our method is rather robust concerning the choice of the parameters. In fact, in most cases the results are better than for the correlation method with optimal window size.

In the second experiment we use a real stereo pair from the INRIA Web site `http://www-sop.inria.fr/robotvis/demo`. In this case the epipolar lines are not parallel to the horizontal axis, and the fundamental matrix is given by

$$F = \begin{bmatrix} 0.000000149 & 0.00000340 & -0.0026 \\ -0.00000718 & 0.00000109 & 0.048 \\ 0.0031 & -0.048 & 1 \end{bmatrix}. \tag{28}$$

TABLE 1
Result of Our Method Applied to the Stereo Pair in Fig. 2

σ_0	σ_n	α	λ_0	s	η	Average error
7	0.8	0.5	−3	0.15	0.95	0.26
10	0.8	0.5	−3	0.15	0.95	0.36
4	0.8	0.5	−3	0.15	0.95	3.23
7	1.0	0.5	−3	0.15	0.95	0.27
7	0.6	0.5	−3	0.15	0.95	0.28
7	0.8	0.6	−3	0.15	0.95	0.27
7	0.8	0.4	−3	0.15	0.95	4.49
7	0.8	0.5	−1	0.15	0.95	0.28
7	0.8	0.5	−5	0.15	0.95	0.58
7	0.8	0.5	−3	0.10	0.95	0.30
7	0.8	0.5	−3	0.20	0.95	0.30
7	0.8	0.5	−3	0.15	0.99	0.30
7	0.8	0.5	−3		0.90	0.33

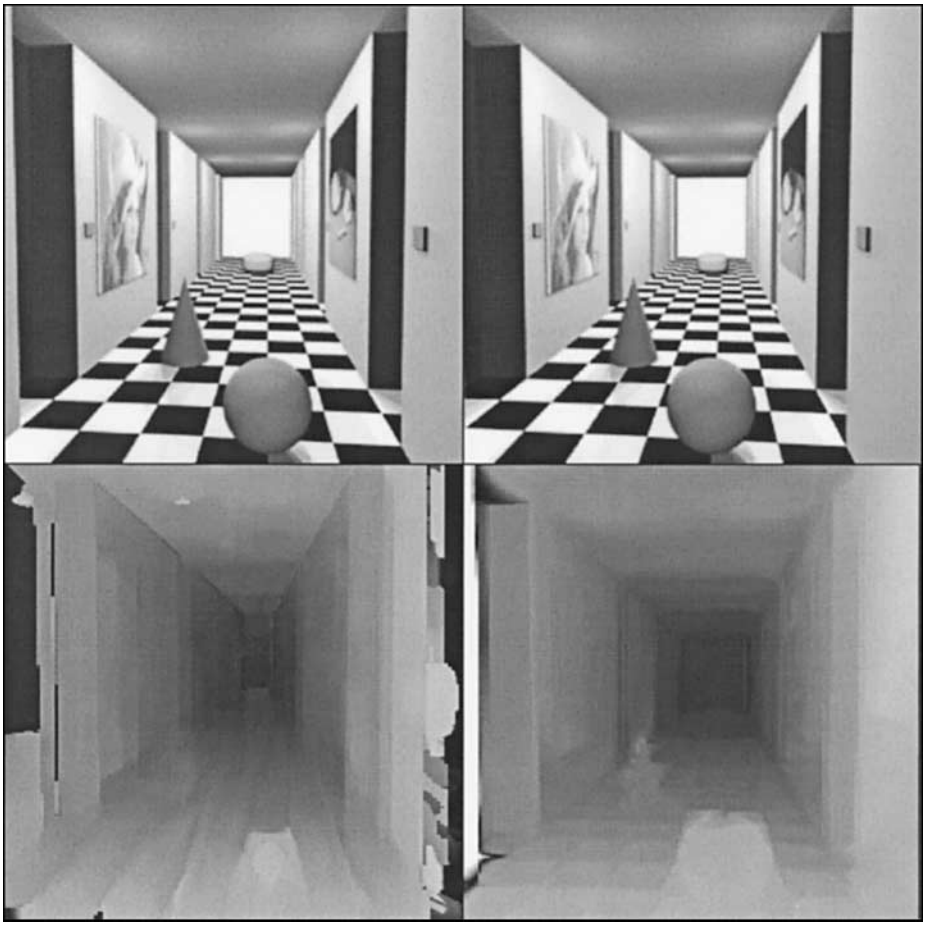

FIG. 2. From left to right and from top to bottom: the original stereo pair, the computed disparity map using a 23 × 23 correlation window, and the disparity map obtained with our method.

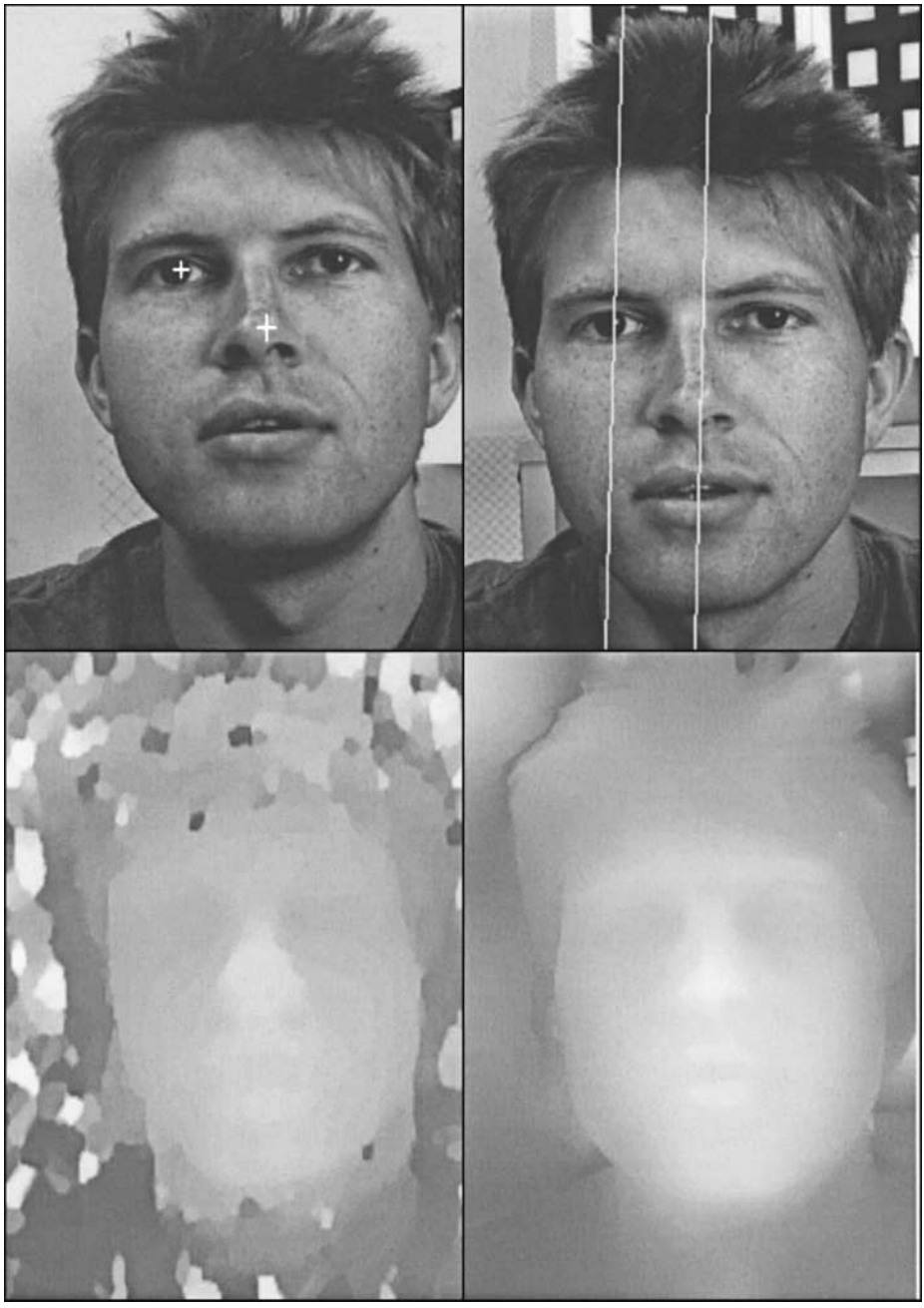

FIG. 3. Top: the original stereo pair. Bottom left: the computed disparity map using a correlation window of size 13×13. Bottom right: our method ($\sigma_0 = 7$, $\sigma_n = 0.8$, $\alpha = 1$, $s = 0.5$, $\eta = 0.95$), with the correlation result as initialization.

In Fig. 3 we present the calculated disparity ($\sqrt{u^2 + v^2}$) using the classical correlation method (bottom left) and using our method with the correlation technique as initialization (bottom right). Two epipolar lines are depicted in the right image. They correspond to the points represented by a cross around the left eye and the nose in the left image. Following

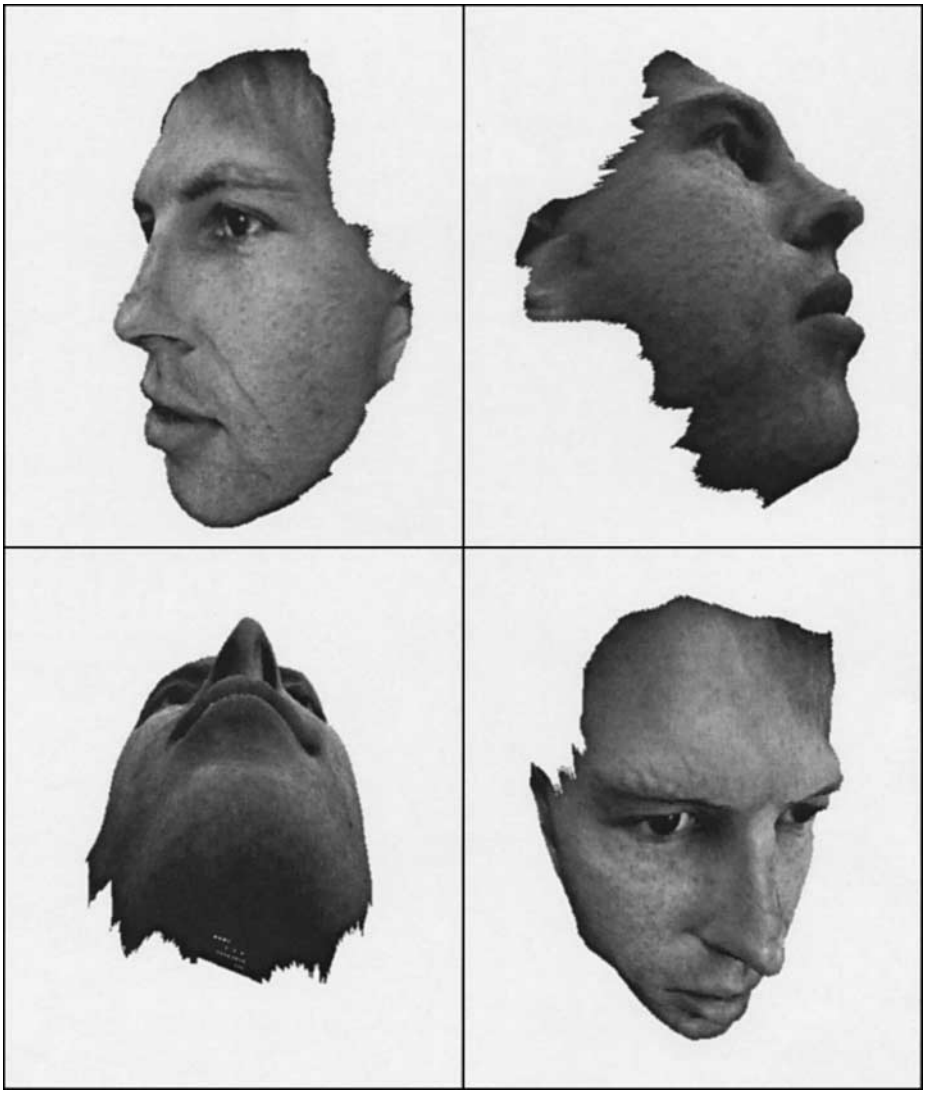

FIG. 4. Four views of the 3-D reconstruction of the stereo pair in Fig. 3, using the disparity map from our method.

the recommendations of one reviewer, the disparity map in the bottom-left part has been postprocessed by a median f lter in order to eliminate erroneous points, followed by morphological closings for f lling holes. Figure 4 shows several views of the 3-D reconstruction of the face in the stereo pair, using the disparity map obtained by our method. The reconstruction looks very realistic.

In Fig. 5 we present an experiment with another stereo pair from the INRIA. It also represents a human face, but the epipolar geometry differs very much from the previous example since the epipolar lines are no longer aligned along the columns as in the previous example. The two epipolar lines in the right image correspond to the two points represented by a cross around the left eye and the nose in the left image. As in the previous example, the disparity map in the bottom-left part has also been postprocessed by a median and a closing process in order to obtain better results. Note that the images are not rectif ed in this

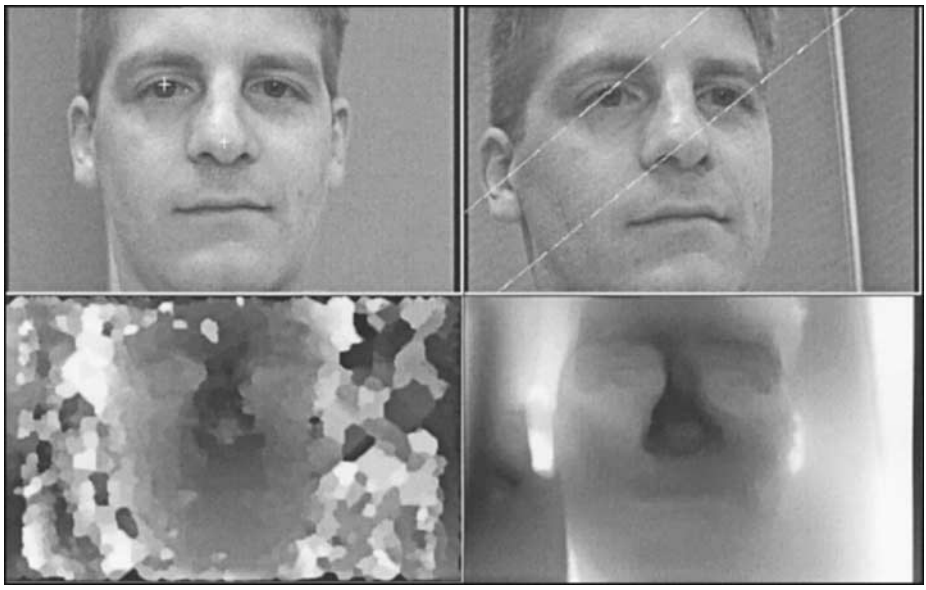

FIG. 5. Top: the original stereo pair. Bottom left: the computed disparity map using a correlation window of size 13×13. Bottom right: our method ($\sigma_0 = 7, \sigma_n = 0.8, \alpha = 1, s = 0.5, \eta = 0.95$), with the correlation result as initialization.

example; i.e., the epipolar lines are not parallel to the columns or the lines of the images. Thus, the disparity map is not simply related to the depth as in the previous example where close points appear brighter and far points darker. The resulting 3-D reconstruction is depicted in Fig. 6. A small artifact, however, becomes visible: because of occlusion problems it is not possible to perfectly reconstruct a region between the left eye and the nose. Here, we can see how the Nagel–Enkelmann smoothness term tries to propagate information from the vicinity in order to keep inconsistencies as small as possible. As a consequence, the eye becomes somewhat extended into the occlusion zone. Larger regions where occlusions make it impossible to obtain a reliable 3-D reconstruction (e.g., the left ear) have been excluded in Fig. 6.

We would like to point out that we have used exactly the same parameter settings in both real-world stereo pairs. In the case of the synthetic pair—where there is no noise present—we have just reduced the values of the isotropy parameter s and the smoothness parameter α. This allows higher discontinuities in the disparity map. In real-world stereo pairs more regularity (i.e., higher values for s and α) is required because of two reasons: first of all, noise is present, and second, in real situations the Lambertian hypothesis about the equal brightness of corresponding image structures is not exactly fulfilled. What is really important is that, even if the number of parameters of the algorithm is high, one can obtain good results in different situations using a default parameter setting. Our experiments illustrate that this even holds for strongly differing epipolar geometries. This again confirms the robustness of the algorithm that we already experienced in Table 1.

More detailed information about the experiments in this section can be found at the Web site `http://serdis.dis.ulpgc.es/~lalvarez/research/demos`. In particular, some movies that illustrate the focusing strategy and the 3-D reconstruction are presented.

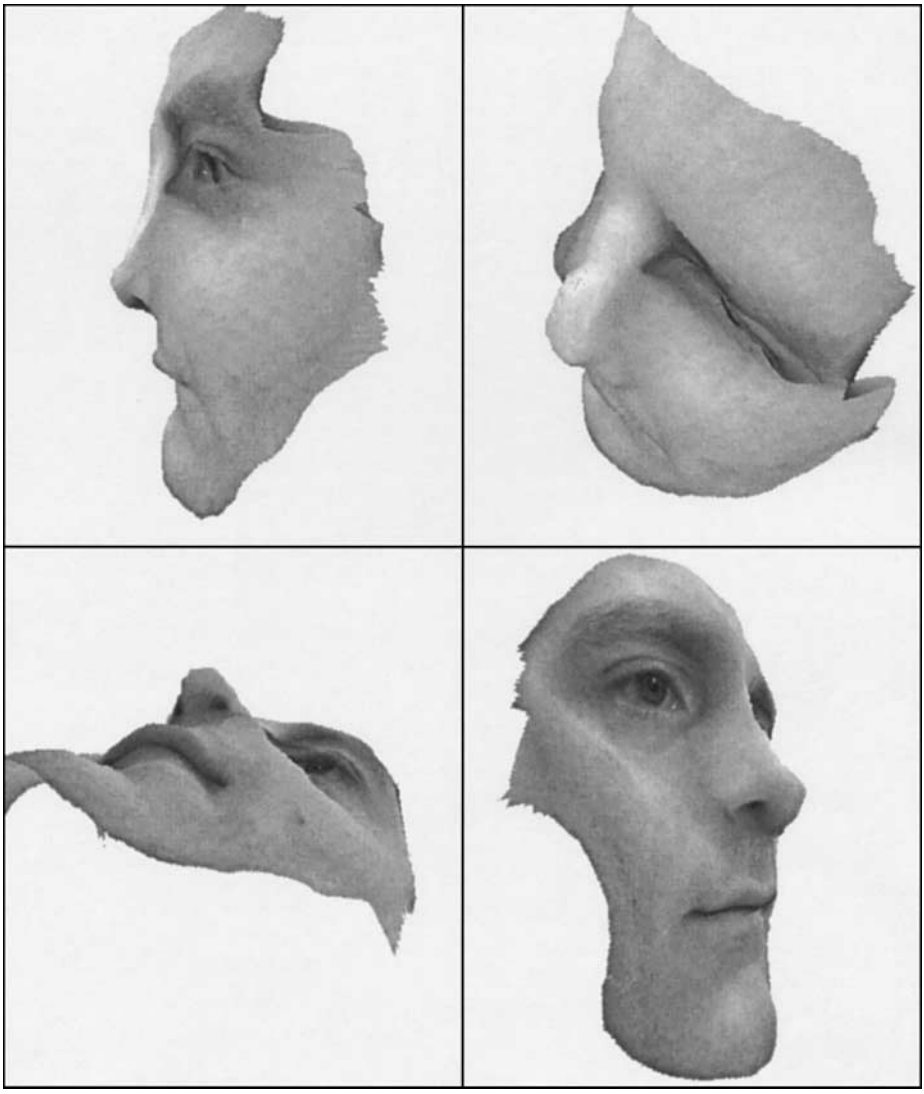

FIG. 6. Four views of the 3-D reconstruction of the stereo pair in Fig. 5, using the disparity map from our method.

5. CONCLUSIONS

The goal of this paper was to present a new energy based method to estimate a dense disparity map between two images. Assuming that the epipolar geometry is known allowed us to simplify the energy model as well as the associated Euler–Lagrange equation. We used a linear implicit f nite difference scheme for its eff cient numerical approximation. In order to avoid that the algorithm converges to physically irrelevant local minima, we embedded it into a linear scale-space approach for focusing the solution from a coarse to a f ne scale.

Our method combines some techniques developed in the context of optic f ow estimation [3, 32] with some other techniques developed in the context of dense disparity map estimation [41] which take into account the geometric constraints associated to a stereo pair. We think that the combination of these ideas is fruitful in that it produces new tools to estimate

dense disparity fields which benefit from the research efforts in stereo vision as well as in optic flow estimation.

The experimental results obtained with our method were very promising. In the case of a synthetic stereo pair, where the exact disparity map is known, we have shown that the results clearly outperform the ones from a classic correlation technique. We have also evaluated our method on two real-world stereo pairs. In this case we have reconstructed the 3-D geometry from the disparity computed with our method. The results obtained here are good as well. Even in occluded regions, where something disappears from one image to the other, artifacts remained moderate thanks to the smoothness term. Here we are currently investigating ways to further improve the results by combining the disparity map information obtained from I_l and I_r with the one from I_r to I_l.

ACKNOWLEDGMENTS

This work has been supported by the European TMR network Viscosity Solutions and their Applications and the Acciones Integradas Proyect HF1998 0098-Project Action Intégrée PICASSO 99050.

REFERENCES

1. L. Alvarez, R. Deriche, J. Sánchez, and J. Weickert, *Dense Disparity Map Estimation Respecting Image Discontinuities: a PDE and Scale-Space Based Approach*, Technical Report INRIA 3874, Sophia–Antipolis, France, 2000.
2. L. Alvarez, P.-L. Lions, and J.-M. Morel, Image selective smoothing and edge detection by nonlinear diffusion, II, *SIAM J. Numer. Anal*. **29**, 1992, 845–866.
3. L. Alvarez, J. Weickert, and J. Sánchez, A scale-space approach to nonlocal optical flow calculations, in *Scale-Space Theories in Computer Vision* (M. Nielsen, P. Johansen, O. F. Olsen and J. Weickert, Eds.), Lecture Notes in Computer Science, Vol. 1682, pp. 235–246, Springer-Verlag, Berlin, 1999.
4. L. Alvarez, J. Weickert, and J. Sánchez, Reliable estimation of optical flow for large displacements, *Internat. J. Comput. Vision* **39**, 2000, 41–56.
5. N. Ayache and C. Hansen, Rectification of images for binocular and trinocular stereovision, in *Ninth International Conference on Pattern Recognition, Beijing, China, Oct. 1988*, pp. 11–16,
6. N. Ayache and F. Lustman, Fast and reliable passive trinocular stereovision, in *Proc. First Int. Conf. on Computer Vision, London, England, June 1987*, pp. 422–427, IEEE Comput. Soc. Press, Los Alamitos, CA.
7. S. T. Barnard, Stochastic stereo matching over scale, *Internat. J. Comput. Vision* **3**, 1989, 17–32.
8. J. L. Barron, D. J. Fleet, and S. S. Beauchemin, Performance of optical flow techniques, *Internat. J. Comput. Vision* **12**, 1994, 43–77.
9. B. Bascle and R. Deriche, Energy based methods for 2D curve tracking, reconstruction, and refinement of 3D curves and applications, in *Geometric Methods in Computer Vision II* (B. C. Vemuri, Ed.), San Diego, CA, July 12–13, SPIE Proceedings, Vol. 2031, pp. 282–293, 1993.
10. A. T. Brint and M. Brady, Stereo matching of curves, *Image Vision Comput*. **8**, 1990, 50–56.
11. R. Deriche, C. Bouvin, and O. Faugeras, A level-set approach for stereo, in *Investigative Image Processing*, (L. I. Rudin and S. K. Bramble, Eds.), Boston, MA, Nov. 1996, SPIE Proceedings, Vol. 2942, pp. 150–161, 1997.
12. R. Deriche, S. Bouvin, and O. Faugeras, Front propagation and level-set approach for geodesic active stereovision, in *Third Asian Conference On Computer Vision*, Hong Kong, January 1998.
13. F. Devernay and O. D. Faugeras, Computing differential properties of 3-D shapes from stereoscopic images without 3-D models, in *Proc. IEEE Conference on Computer Vision and Pattern Recognition*, Seattle, WA, June 21–23, 1994, pp. 208–213.
14. W. Enkelmann, Investigation of multigrid algorithms for the estimation of optical flow fields in image sequences, *Comput. Vision Graphics Image Process*. **43**, 1988, 150–177.
15. O. Faugeras, *Three-Dimensional Computer Vision: a Geometric Viewpoint*, MIT Press, Cambridge, MA, 1993.

16. O. Faugeras, B. Hotz, H. Mathieu, T. Viéville, Z. Zhang, P. Fua, E. Théron, L. Moll, G. Berry, J. Vuillemin, P. Bertin, and C. Proy, Real time correlation based stereo: algorithm implementations and applications. *Internat. J. Comput. Vision*, to appear.
17. O. Faugeras and R. Keriven, Variational principles, surface evolution, PDE's, level set methods and the stereo problem, *IEEE Trans. Image Process.* **7**, 1998, 336–344.
18. D. J. Fleet and A. D. Jepson, Computation of component image velocity from local phase information, *Internat. J. Comput. Vision* **5**, 1990, 77–104.
19. D. J. Fleet and A. D. Jepson, Stability of phase information, *IEEE Trans. Pattern. Anal. Mach. Intell*. **15**, 1993, 1253–1268.
20. L. Florack, *Image Structure*, Kluwer, Dordrecht, 1997.
21. P. Fua, A parallel stereo algorithm that produces dense depth maps and preserves image features, *Mach. Vision Appl*. **6**, 1993, 35–49. [Available as INRIA Research Report 1369]
22. W. E. L. Grimson, Computational experiments with a feature based stereo algorithm, *IEEE Trans. Pattern Anal. Mach. Intell*. **7**, 1985, 17–34. [See also MIT Memo 762, January 1984.]
23. F. Heitz, P. Pérez, and P. Bouthemy, Multiscale minimization of global energy functions in some visual recovery problems, *CVGIP: Image Understanding* **59**, 1994, 125–134.
24. T. Iijima, Basic theory on normalization of pattern (in case of typical one-dimensional pattern), *Bull. Electrotech. Lab*. **26**, 1962, 368–388. [In Japanese]
25. M. R. M. Jenkin and A. D. Jepson, Recovering local surface structure through local phase difference methods, *CVGIP: Image Understanding* **59**, 1994, 72–93.
26. D. G. Jones and J. Malik, A computational framework for determining stereo correspondence from a set of linear spatial filters, in *Computer Vision-ECCV '92* (G. Sandini, Ed.), Lecture Notes in Computer Science, Vol. 588, pp. 395–410, Springer-Verlag, Berlin, 1992.
27. C. D. Kuglin and D. C. Hines, The phase correlation image alignment method, in *Conference on Cybernetics and Society*, New York, Sept. 1975, pp. 163–165.
28. T. Lindeberg, A scale selection principle for estimating image deformations, *Image Vision Comput*. **16**, 1998, 961–977.
29. J. H. McIntosh and K. M. Mutch, Matching straight lines, *Comput. Vision Graphics Image Process*. **43**, 1998, 386–408.
30. G. Medioni and R. Nevatia, Segment based stereo matching, *Comput. Vision Graphics Image Process*. **31**, 1985, 2–18.
31. H.-H. Nagel, Constraints for the estimation of displacement vector fields from image sequences, in *Proc. Eighth Int. Joint Conf. on Artificial Intelligence*, Karlsruhe, Germany, Aug. 8–12, 1983, pp. 945–951.
32. H.-H. Nagel and W. Enkelmann, An investigation of smoothness constraints for the estimation of displacement vector fields from images sequences, *IEEE Trans. Pattern Anal. Mach. Intell*. **8**, 1986, 565–593.
33. N. M. Nasrabadi, A stereo vision technique using curve-segments and relaxation matching, *IEEE Trans. Pattern Anal. Mach. Intell*. **14**, 1992, 566–572.
34. M. Nielsen and R. Deriche, Binocular dense depth reconstruction using isotropy constraint, in *Theory and Applications of Image Processing II* (G. Borgefors, Ed.), pp. 127–140, World Scientific, Singapore, 1995.
35. M. Nielsen, R. Maas, W. J. Niessen, L. M. J. Florack, and B. M. ter Haar Romeny, Binocular stereo from grey-scale images, *J. Math. Imag. Vision* **10**, 1999, 103–122.
36. K. Nishihara, Practical real-time imaging stereo matcher, *Opt. Engineering* **23**, 1984, 536–545. [See also MIT AI MEMO-772, Aug. 1984]
37. Y. Ohta and T. Kanade, Stereo by intra- and inter-scanline search, *IEEE Trans. Pattern Anal. Mach. Intell.* **7**, 1985, 139–154.
38. S. B. Pollard, J. E. W. Mayhew, and J. P. Frisby, PMF: a stereo correspondence algorithm using a disparity gradient constraint, *Perception* **14**, 1985, 449–470.
39. M. Pollefeys, R. Koch, and L. Van Gool, A simple and efficient rectification method for general motion, in *Proc. 7th Int. Conf. on Computer Vision*, Corfu, Greece, Sept. 21–24, 1999, pp. 496–501, IEEE Comput. Soc. Press, Los Alamitos, CA.
40. M. Proesmans, E. Pauwels, and L. Van Gool, Coupled geometry-driven diffusion equations for low-level vision, in *Geometry-Driven Diffusion in Computer Vision* (B. M. ter Haar Romeny, Ed.), pp. 191–228, Kluwer, Dordrecht, 1994.

41. L. Robert and R. Deriche, Dense depth map reconstruction: a minimization and regularization approach which preserves discontinuities, in *Computer Vision-ECCV '96* (B. Buxton and R. Cipolla, Eds.), Vol. I, pp. 439–451, Lecture Notes in Computer Science, Vol. 1064, Springer-Verlag, Berlin, 1996.
42. L. Robert, R. Deriche, and O. D. Faugeras, Dense depth recovery from stereo images, in *Proc. European Conf. on Artificial Intelligence*, Vienna, Austria, Aug. 1992, pp. 821–823.
43. L. Robert and O. Faugeras, Curve-based stereo: f gural continuity and curvature, in *Proc. Int. Conf. on Computer Vision and Pattern Recognition*, Lahaina, Hawai, June 3–6, 1991, pp. 57–62, IEEE Comput. Soc. Press, Los Alamitos, CA.
44. S. Roy, J. Meunier, and I. Cox, Cylindrical rectif cation to minimize epipolar distortion, in *Proc. Int. Conf. on Computer Vision and Pattern Recognition*, San Juan, Puerto Rico, June 17–19, 1997, pp. 393–399, IEEE Comput. Soc. Press, Los Alamitos, CA.
45. C. Schnörr, Determining optical f ow for irregular domains by minimizing quadratic functionals of a certain class, *Internat. J. Comput. Vision* **6**, 1991, 25–38.
46. J. Shah, A nonlinear diffusion model for discontinuous disparity and half-occlusions in stereo, in *Proc. Int. Conf. on Computer Vision and Pattern Recognition*, New York, June 15–17, 1993, pp. 34–40, IEEE Comput. Soc. Press, Los Alamitos, CA.
47. M. A. Snyder, On the mathematical foundations of smoothness constraints for the determination of optical f ow and for surface reconstruction, *IEEE Trans. Pattern Anal. Mach. Intell*. **13**, 1991, 1105–1114.
48. J. Sporring, M. Nielsen, L. Florack, and P. Johansen (Eds.), *Gaussian Scale-Space Theory*, Kluwer, Dordrecht, 1997.
49. J. Weickert, Theoretical foundations of anisotropic diffusion in image processing, *Comput. Suppl*. **11**, 1996, 221–236.
50. J. Weickert, *Anisotropic Diffusion in Image Processing*, Teubner, Stuttgart, 1998.
51. J. Weickert, S. Ishikawa, and A. Imiya, Linear scale-space has f rst been proposed in Japan, *J. Math. Imag. Vision* **10**, 1999, 237–252.
52. J. Wiklund, C. J. Westelius, and H. Knutsson, Hierarchical phase based disparity estimation, in *Proc. Second Int. Singapore Conf. on Image Processing* (V. Srinivasan, Ong. S. H. and Ang Y. H., Eds.), Singapore, Sept. 7–11, 1992, pp. 128–131.
53. N. Yokoya, *Stereo Surface Reconstruction by Multiscale-Multistage Regularization*, Technical Report TR-90-45, Electrotechnical Laboratory, Tsukuba, Japan, Nov. 1990.
54. C. Zeller and O. Faugeras, Applications of non-metric vision to some visually guided tasks, in *Proc. Int. Conf. on Pattern Recognition*, Jerusalem, Israel, Oct. 1994, pp. 132–136, IEEE Comput. Soc. Press, Los Alamitos, CA. [Longer version available as INRIA Research Report RR2308]

LUIS ALVAREZ received a M.Sc. in applied mathematics in 1985 and a Ph.D. in mathematics in 1988, both from Complutense University (Madrid, Spain). Between 1991 and 1992 he worked as a post-doctoral researcher at CEREMADE, Université Paris IX–Dauphine (France). Currently he is with the Computer Science Department of the University of Las Palmas de Gran Canaria. His research interests are computer vision and partial differential equations. He is the scientif c leader of the computer vision group of the University of Las Palmas named AMI (see the Web site http://amiserver.dis.ulpgc.es/ami for more details).

RACHID DERICHE graduated from the Ecole Nationale Supérieure des Télécommunications, Paris, in 1979 and received the Ph.D. in mathematics from the University of Paris XI, Dauphine in 1982. He is currently a research director at INRIA Sophia-Antipolis in the Computer Vision and Robotics Group. His research interests are in computer vision and image processing and include partial differential equations applied to image processing and computer vision, low-level vision, motion analysis and visual tracking, calibration and stereo, and image sequence analysis. More generally, he is very interested in the application of mathematics to computer vision and image processing. He has authored or co-authored over 100 scientif c papers. To f nd out more about his research and some selected publications take a look at his Web page under the address http://www-sop.inria.fr/robotvis/personnel/der/der-eng.html.

JAVIER SÁNCHEZ received a M.Sc. in computer science in 1997 from the University of Las Palmas de Gran Canaria. Between October 1997 and February 1998, he obtained an ERASMUS grant to follow some courses of the DEA 127 "Informatique: Systèmes Intelligents" at the University of Paris IX–Dauphine. Currently, he holds a grant from the Computer Science Department of the University of Las Palmas where he is working on his doctoral thesis under the direction of Professor Luis Alvarez.

JOACHIM WEICKERT obtained a M.Sc. in industrial mathematics in 1991 and a Ph.D. in mathematics in 1996, both from Kaiserslautern University (Germany). From 1996 to 1998 he worked as a postdoctoral researcher at the universities of Utrecht (The Netherlands) and Copenhagen (Denmark). Currently he is assistant professor at the Computer Vision, Graphics, and Pattern Recognition Group of the University of Mannheim (Germany). His scientif c interests include image processing, computer vision, partial differential equations, and scientif c computing. Joachim Weickert received the 1993 Wacker Memorial Prize and the 1998 Olympus Research Award, and he authored the book *Anisotropic Diffusion in Image Processing* (Teubner, Stuttgart, 1998).